Cancer Letters 642 (2026) 218247

Contents lists available at ScienceDirect

Cancer Letters

journal homepage: www.elsevier.com/locate/canlet

Original Articles

# *Ganoderma lucidum* polysaccharide ameliorates cancer cachexia with enhanced efficacy in aged group by reprogramming arginine metabolism to modulate Treg formation

Chunmiao Deng [a,1], Yunfang Chen [b,1], Jiaojiao Xu [c,1], Chanjin Liang [d], Cui Shao [e], Shiqi Mei [d], Yongkang Xu [f], Yin Li [e], Cancan Zheng [a,*], Yichang Luo [e,**], Xingyuan Shi [d,***]

[a] State Key Laboratory of Respiratory Disease, Key Laboratory of Biological Targeting Diagnosis, Therapy and Rehabilitation of Guangdong Higher Education Institutes, The Fifth Affiliated Hospital of Guangzhou Medical University, Guangzhou, China
[b] Department of Scientific Research and Teaching, Shenzhen People's Hospital (The First Affiliated Hospital, Southern University of Science and Technology; the Second Clinical Medical College, Jinan University), Shenzhen, China
[c] State Key Laboratory of Respiratory Disease, Guangdong Provincial Key Laboratory of Protein Modification and Degradation, School of Basic Medical Sciences, Guangzhou Medical University, Guangzhou, China
[d] Department of Radiation Oncology, The Fifth Affiliated Hospital of Guangzhou Medical University, Guangzhou, Guangdong, China
[e] The Affiliated Traditional Chinese Medicine Hospital, Sleep Research Institute of Traditional Chinese Medicine, Guangzhou Medical University, Guangzhou, China
[f] GuangZhou ShanYuanTang Health Science and Technology Co., LTD, Factory 101. No.10. Yuexiu Industrial Park Street, Outline Ridge Village, Zhongluotan Town, Baiyun District, Guangzhou, China

ARTICLE INFO

*Keywords:*
*Ganoderma lucidum* polysaccharides
Cancer cachexia
Aging
Muscle atrophy
Dyslipolysis
Immunomodulation

ABSTRACT

Cancer cachexia is a syndrome characterized by profound weight loss, muscle wasting, and metabolic disturbance in cancer patients. Cancer-associated cachexia represents significant biological and clinical challenges that profoundly affect human health. Approximately 20 % of cancer patients succumb directly to cachexia-related complications. Aging is characterized by a gradual decline in physiological functions and an increased vulnerability to chronic diseases. However, whether aging inherently increases vulnerability to cachexia or exacerbates its progression remains unclear, impeding the development of targeted strategies for this high-risk population. *Ganoderma lucidum* polysaccharides (GLP) have demonstrated diverse pharmacological activities; however, their potential role in attenuating of tumor cachexia remains inadequately explored and warrants further investigation. In this study, GLP was found to mitigate tumor cachexia *in vitro* and *in vivo* models, as evidenced by rescuing significant weight loss, muscle atrophy, and adipose tissue breakdown. Notably, its therapeutic potency is more profoundly marked in aged mice than in young ones. Mechanistically, GLP alleviated myofiber atrophy and dyslipolysis by inactivating NF-κB and AMPK pathways, while also activating Treg cells by regulating arginine metabolism. In conclusion, our findings indicate that GLP exhibits cachexia-attenuating activities, thereby positioning it as a potential therapeutic candidate for aging-related conditions.

## 1. Introduction

Lung cancer is the leading cause of cancer incidence and mortality in China, profoundly impacting public health [1]. Cancer-associated cachexia, a complex multifactorial syndrome affecting multiple organ systems, is a major contributor to morbidity and mortality in individuals with lung cancer [2]. Cachexia is characterized not only by significant weight loss but also by muscle atrophy, abnormal adipose tissue breakdown, and metabolic disorders [3,4]. The pathogenesis of cachexia is multifaceted, involving inflammatory responses, metabolic abnormalities, endocrine changes, and tumor-host interactions. Excessive release of inflammatory factors is a key characteristic of cachexia. These

* Corresponding author. Department of Radiation Oncology, The Fifth Affiliated Hospital of Guangzhou Medical University, Guangzhou, China.
** Corresponding author.
*** Corresponding author. State Key Laboratory of Respiratory Disease, Key Laboratory of Biological Targeting Diagnosis, Therapy and Rehabilitation of Guangdong Higher Education Institutes, The Fifth Affiliated Hospital of Guangzhou Medical University, Guangzhou, China.
*E-mail addresses:* zcchpl@163.com (C. Zheng), 546176703@qq.com (Y. Luo), 18549183@qq.com (X. Shi).
[1] These authors contributed equally to this manuscript.

https://doi.org/10.1016/j.canlet.2026.218247
Received 12 September 2025; Received in revised form 2 January 2026; Accepted 6 January 2026
Available online 7 January 2026

factors, including tumor necrosis factor-alpha (TNF-α) and interleukin-6 (IL-6), play crucial roles in promoting the breakdown of muscle and fat. Additionally, tumor tissues can secrete various factors that directly affect metabolic balance and may exacerbate cachexia by altering the host's immune response [5]. Clinically, cancer-associated cachexia not only impairs the patients' tolerance to chemotherapy and radiotherapy but is also often linked to poor survival [6,7]. However, effective treatments for cachexia remain limited, primarily focusing on nutritional support and symptomatic management. Therefore, in-depth research on the pathogenesis of lung cancer cachexia and the development of novel treatment strategies are crucial for improving patient prognosis and quality of life.

Aging is a potent driver of cancer vulnerability, with incidence escalating proportionally to age. This process fundamentally disrupts cellular metabolism, immune competence, and nutrient-sensing networks, thereby intensifying treatment resistance and comorbidity severity in elderly cancer patients [8]. In cancer patients, cachexia and sarcopenia frequently coexist. Both represent systemic syndromes characterized by complex interactions across multiple organ systems, ultimately contributing to chronic inflammation and metabolic dysregulation [9]. Age-associated Tregs accumulation correlates with impaired cytotoxic lymphocyte infiltration and accelerated cachexia progression, highlighting immune dysregulation as a critical axis linking senescence to cancer aggressiveness [10]. Understanding this interplay is critical for developing targeted strategies to mitigate cachexia in older cancer patients. The strategy of eliminating senescent cells or reducing the production and secretion of senescence-associated secretory phenotype factors is a promising anti-aging approach for cancer treatment [11–13].

As an ancient Chinese medicine, *Ganoderma lucidum* has long been regarded as a “superior herb” and has been extensively studied for its diverse pharmacological effects [14], including immunomodulatory [15], antioxidant [16], anti-inflammatory [17], and antitumor [18,19]. As the primary active constituents of *Ganoderma lucidum*, the effect of *Ganoderma lucidum* polysaccharides (GLP) on tumor cachexia and its underlying mechanisms remains unclear. In this study, we aim to clarify the key link between aging and cachexia, dissect the role of immune regulation in this interplay, and propose GLP as an effective therapeutic agent for cancer cachexia.

## 2. Results

### 2.1. GLP alleviates cancer cachexia in the xenograft model and demonstrates enhanced efficacy in the aged mice

The mechanistic link between aging and cachexia remains largely unknown. By analyzing clinical data of 40 patients with cancer cachexia [20], we found that compared to patients aged <65 years, those aged ≥65 years exhibited more significant weight loss over the past six months, suggesting that the aging population has an increased susceptibility to cachexia (Fig. 1A). To further investigate the correlation between aging and cancer cachexia, we developed a xenograft mouse model via the subcutaneous injection of Lewis lung carcinoma (LLC) cells. We involved both young and aged mice, then exposed to GLP treatment, respectively (Fig. 1B). Observations of physiological parameters in LLC tumor-bearing mice indicated that, as illustrated in Fig. 1C, the body weight of healthy control mice increased consistently throughout the experiment. In contrast, the body weight of LLC tumor-bearing mice demonstrated a declining trend. Notably, administration of GLP (10 mg/kg) effectively mitigated this weight loss, while maintaining an unchanged tumor size (Supplementary Fig. 1A–D). More interestingly, exposure to GLP induced a more profound change in aged mice than in young ones (Fig. 1D). Additionally, by monitoring the food intake, we noted that the food take of GLP-treated aged mice was essentially consistent with that of the healthy group, indicating that GLP treatment restored the food intake of aged mice to a level closer to that of the healthy group (Fig. 1E). Blood cell analyses of mice revealed that GLP effectively counteracted the decrease in lymphocyte proportion associated with LLC tumor cachexia and normalized the elevated neutrophil levels induced by LLC tumor cachexia in both young and aged mice (Supplementary Fig. 1E–F). These findings collectively suggest that GLP effectively relieves cancer cachexia and exhibits improved efficacy in aged mice. Additionally, the toxic effects of GLP were evaluated in mice. Measurements of white blood cell count (WBC), red blood cell count (RBC), hemoglobin (HGB), and platelet count (PLT) revealed no significant differences among the groups (Supplementary Fig. 2A). Histological analysis demonstrated that GLP treatment was not toxic to major organs, including the liver, kidneys, and spleen (Supplementary Fig. 2B). Collectively, these findings indicate that GLP possesses a favorable safety profile.

### 2.2. GLP relieves muscle atrophy by inactivating the NF-κB signaling pathway

We next investigated the effects of GLP on cachexia by constructing an *in vitro* cachexia model utilizing C2C12 myoblasts (Fig. 2A). First, we assessed the cytotoxicity of GLP towards C2C12 cells, and the results indicated that GLP exhibits minimal toxicity to the cells at concentrations below 10 μg/mL (Supplementary Fig. S3A). Subsequently, we evaluated the protective effects of GLP on C2C12 myotubes in the presence of conditioned medium (CM) from LLC cells or colorectal adenocarcinoma cells (CT26), respectively. As illustrated in Fig. 2B, the application of LLC and CT26-derived CM induced significant atrophy of C2C12 myotubes. In contrast, GLP exerted a dose-dependent protective effect against atrophy of myotubes induced by cancer cells, suggesting that GLP may have potential therapeutic value for mitigating cachexia-related muscle wasting. Muscle-specific E3 ubiquitin ligases, particularly muscle RING finger protein 1 (MuRF1) and F-box protein 32 (Atrogin-1), play a critical role in muscle degradation [21]. The results from Quantitative real-time PCR (qRT-PCR) and Western blot demonstrated that the LLC or CT26-derived CM significantly upregulated the expression levels of MuRF1 and Atrogin-1, while GLP treatment effectively reversed this increase. These E3 ubiquitin ligases have been reported to facilitate muscle atrophy by degrading myosin and myogenic transcription factors [22]. We indeed observed that cancer cell-induced myotube atrophy was accompanied by a marked reduction in the expression of myosin heavy chain (MyHC) and the myogenic transcription factor MyoD1. Notably, GLP reversed these effects in a dose-dependent manner (Fig. 2C–D). In addition, muscle cell senescence is a crucial indicator of muscle atrophy. To investigate the effect of GLP on muscle aging, we conducted β-galactosidase staining and found that the CM from cancer cells induces senescence in C2C12 cells, whereas the effect was abolished in the presence of GLP (Fig. 2E). Additionally, Western blot analysis of the senescence marker LaminB1 yielded consistent results (Fig. 2F). Recent research has identified NF-κB as a crucial signaling pathway involved in cancer-induced muscle atrophy [23]. Our Western blot assay also confirmed that LLC or CT26-derived CM can activate the NF-κB signaling. Furthermore, treatment with GLP significantly inhibited the activation of the NF-κB pathway (Fig. 2G) and the nuclear translocation of p65 (Fig. 2H). To further investigate the mechanism behind the protective effects of GLP on myofiber atrophy and its potential dependency on the NF-κB pathway, we examined the expression of key pro-inflammatory cytokines commonly associated with muscle wasting, including IFN-γ, IL-6, and TNF-α. The results of ELISA indicated that GLP treatment inhibits the expression of IFN-γ, IL-6, and TNF-α in aged mice, providing insight into the mechanism behind its more profound effects in this population (Supplementary Fig. S3B).

### 2.3. Protective effects of GLP on myofiber atrophy in vivo

By establishing the tumor xenograft model in young or old mice, we

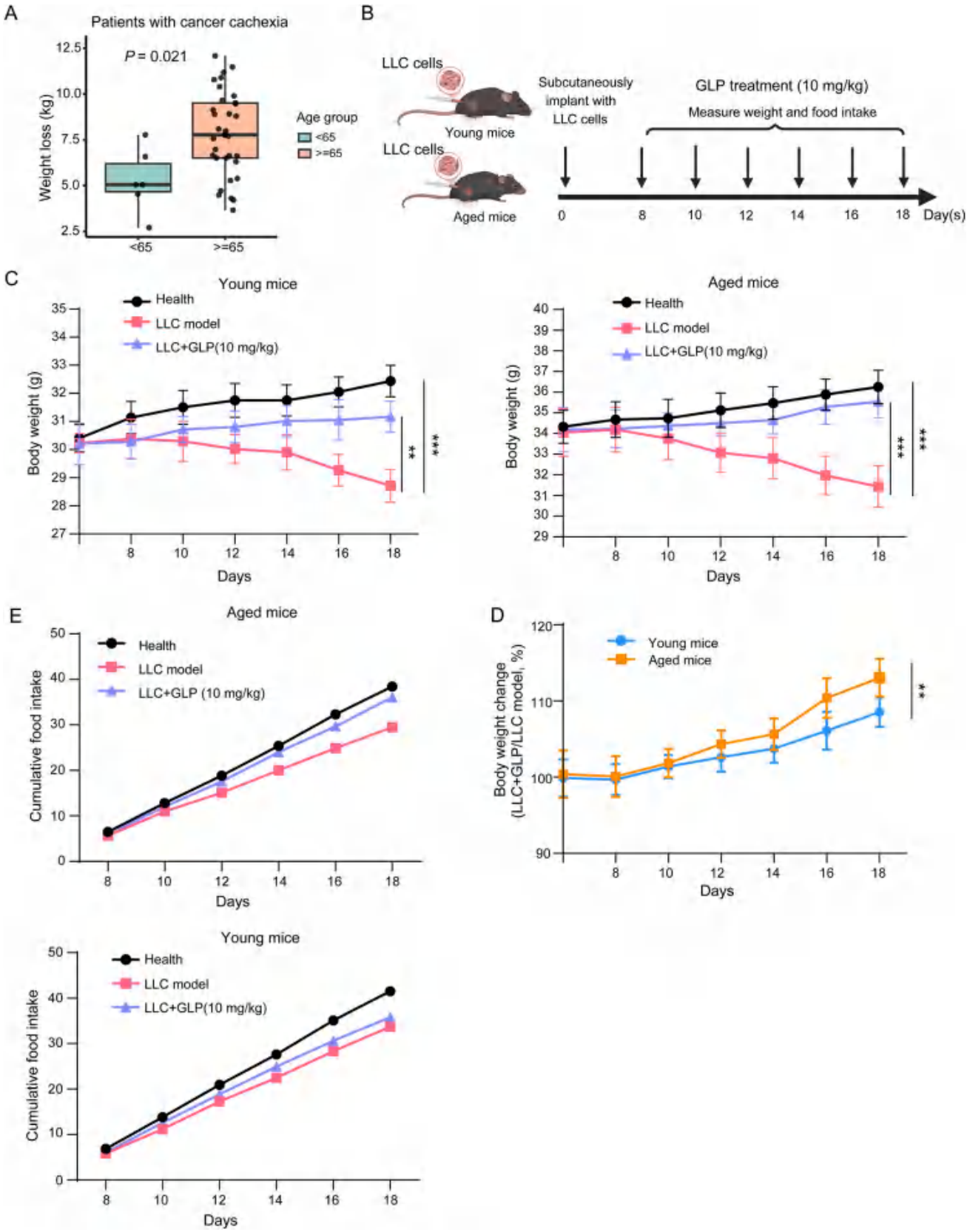


**Fig. 1.** GLP attenuated cachexia symptoms of mice challenged with LLC tumors. (A) The bar chart comparing the weight loss between patients aged >65 years and those aged<65 in a cohort of 40 individuals with cancer cachexia. (B) The diagram showing the mouse model design (n = 6). (C) Changes in body weight of mice with or without LLC tumor implantation and following GLP treatment in the young or aged mice, respectively. (D) The body weight change between young and aged mice. (E) Cumulative food intake of mice in the presented groups was measured throughout the experimental period. Data are presented as mean ± SD. **, $P < 0.01$; ***, $P < 0.001$; ns, no significant difference.

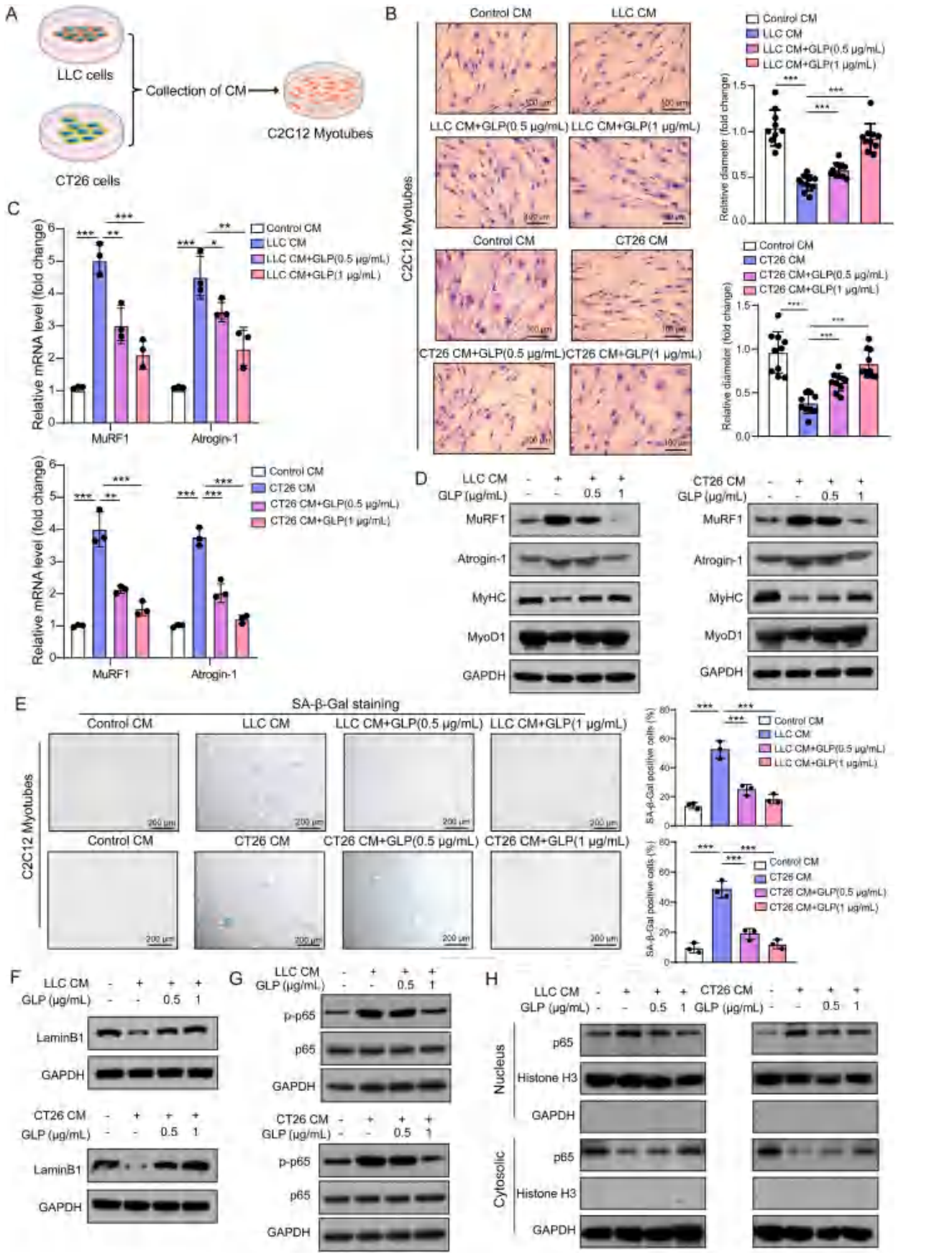


*(caption on next page)*

**Fig. 2.** Effects of GLP on C2C12 myotube atrophy and senescence *in vitro*. (A) The diagram illustrating the cell model design. (B) Representative morphology of C2C12 myotubes subjected to LLC or CT26 cells-CM with or without GLP treatment; scale bar = 100 μm. (C) qRT-PCR analysis of MuRF1 and Atrogin-1 mRNA expression levels in C2C12 myotubes following induction with LLC or CT26-derived CM, with or without GLP treatment. (D) Western blot analysis of MuRF1, Atrogin-1, MyHC, and MyoD1 protein levels in C2C12 myotubes treated with LLC or CT26-derived CM in the presence or absence of GLP. (E) Senescence-associated β-galactosidase (SA-β-Gal) staining indicating the effect of GLP on cellular senescence in C2C12 myotubes; scale bar = 200 μm. (F–G) Western blot analysis of LaminB1 (F), phosphorylated p65 (p-p65) and total p65 (G) protein levels in C2C12 myotubes treated with LLC or CT26-derived CM, with or without GLP treatment. (H) Nuclear and cytoplasmic distribution of p65 in C2C12 cells treated with LLC or CT26-derived CM in the presence or absence of GLP. Data are presented as mean ± SD. *, $P < 0.05$; **, $P < 0.01$; ***, $P < 0.001$.

further measured the physiological parameters of the gastrocnemius (GA) muscle in LLC tumor-bearing mice, indicative of muscle atrophy. The results indicated that LLC tumors caused a significant decrease in GA muscle mass, whereas treatment with GLP (10 mg/kg) effectively reversed this loss (Fig. 3A). Notably, the therapeutic effect of GLP was more pronounced in aged mice (Fig. 3B). Hematoxylin and eosin (H&E) staining of the GA muscle revealed a significant reduction in the cross-sectional area (CSA) of GA myofibers in LLC tumor-bearing mice. In contrast, GLP treatment effectively ameliorated this shrinkage (Fig. 3C). Furthermore, by checking the GA muscle tissues, Western blot analysis revealed that the protein levels of MyHC and MyoD1 were decreased in the LLC group, the presence of GLP significantly reversed the decreases in MyHC and MyoD1 (Fig. 3D). In contrast, muscle-specific E3 ubiquitin ligases (including MuRF1 and Atrogin-1) were significantly increased in LLC tumor-bearing mice, while GLP treatment partially ameliorated the upregulation of these two ligases in the GA muscle tissues (Fig. 3D–E). Consistently, the activation of NF-κB signaling in the GA muscle tissues of LLC tumor model mice was partially inhibited by GLP (Fig. 3F). Taken together, these results demonstrated that LLC tumor-induced cachexia led to muscle atrophy in mice, while treatment with GLP effectively alleviated cachexia-associated muscle atrophy by inactivating NF-κB signaling, with a more pronounced therapeutic effect observed in aged mice.

### 2.4. GLP suppresses lipolysis by modulating AMPK and fatty acid β-oxidation pathways in vitro

In addition to muscle atrophy, a significant portion of weight loss in patients with cancer cachexia stems from the depletion of adipose tissue. To investigate the effects of GLP on fat metabolism, we first induced the differentiation of 3T3-L1 precursor adipocytes into mature adipocytes using differentiation medium. We next assessed the cytotoxicity of GLP toward 3T3-L1 adipocytes and noted that GLP exerted no cytotoxic effects on these cells at doses lower than 5 μg/mL (Supplementary Fig. 4A–B). Results from Oil Red O staining revealed that mature 3T3-L1 adipocytes treated with LLC or CT26-derived CM contained fewer lipid droplets compared to control cells. In contrast, treatment with GLP resulted in a dose-dependent increase in the number of lipid droplets (Fig. 4A). Hormone-sensitive lipase (HSL), a key triglyceride lipase predominantly expressed in adipose tissue, has been reported to play essential roles in energy homeostasis [24]. In mature 3T3-L1 adipocytes exposed to LLC or CT26-derived CM, the phosphorylation of HSL was significantly upregulated; however, this upregulation was effectively reversed by treatment with GLP (Fig. 4B).

To elucidate the underlying mechanism, we investigated the involvement of AMPK signaling, a key upstream pathway that regulates HSL phosphorylation and energy balance, in this process of lipolysis. Our findings indicated that GLP treatment significantly inhibited the phosphorylation of AMPKα (Fig. 4B). Furthermore, to determine whether abnormal fat metabolism associated with cancer cachexia is linked to decreased adipogenesis and increased fatty acid β-oxidation, we measured mRNA expression levels of genes related to adipogenesis and fatty acid β-oxidation pathways in 3T3-L1 adipocytes using qRT-PCR. The results indicated that LLC or CT26-derived CM significantly inhibited the expression of lipogenic genes, including FASN, ACC1, and SCD1, while simultaneously increasing the expression of genes associated with fatty acid β-oxidation, specifically ACOX1 and CPT2. Although treatment with GLP effectively reversed the expression of genes related to fatty acid β-oxidation, it did not significantly affect the expression of genes involved in lipogenesis (Fig. 4C–E). Overall, these findings indicated that GLP can inhibit lipolysis by suppressing AMPK signaling and the fatty acid β-oxidation pathways. Additionally, we assessed the expression of adipose triglyceride lipase (ATGL), a key enzyme involved in lipolysis, and the activation status of the PKA/CREB pathway, which plays a crucial role in regulating lipolysis. Western blot analysis revealed that GLP treatment significantly suppressed the expression of ATGL and inhibited the activation of the PKA/CREB pathway. These results further support the notion that GLP exerts its protective effects against cachexia-induced fat loss by modulating key lipid metabolism pathways, including the inhibition of lipolysis through the AMPK and PKA/CREB signaling pathways (Fig. 4F).

### 2.5. Epididymal white adipose tissue homeostasis is enhanced by GLP through the modulation of AMPK signaling and fatty acid β-oxidation in mice

We further assessed the epididymal white adipose tissue (eWAT) in mice with LLC-derived xenografts, and the results revealed a significant decrease in eWAT weight in the LLC tumor model (Fig. 5A–B). Consistently, the cross-sectional area of adipocytes in eWAT tissues was also reduced in LLC tumor-bearing mice. Treatment with GLP effectively ameliorated the reductions in both eWAT weight and adipocyte cross-sectional area, demonstrating more pronounced therapeutic effects in aged mice (Fig. 5C). Furthermore, we investigated whether GLP regulated adipose tissue homeostasis in cachectic mice by modulating the AMPK and fatty acid β-oxidation pathways. Consistent with our *in vitro* experiments, increased phosphorylation of AMPKα was detected in the eWAT of mice bearing LLC tumors, indicating activation of the AMPK signaling pathway (Fig. 5D). Additionally, the phosphorylation of HSL was also elevated in the eWAT of these mice. In contrast, GLP treatment significantly inhibited both the activation of the AMPK pathway and the phosphorylation of HSL (Fig. 5D). This observation correlated with reduced serum triglyceride (TG) levels, primary substrates for HSL, in LLC tumor-bearing mice, which were partially restored by GLP treatment (Fig. 5E). Moreover, the expression of ACOX1 and CPT2, both associated with fatty acid β-oxidation, was upregulated in the LLC tumor model group, indicating an accelerated rate of fatty acid β-oxidation in the eWAT of mice with LLC tumors. Notably, GLP treatment partially reversed these changes in gene expression (Fig. 5F). Collectively, these results suggest that GLP treatment may ameliorate eWAT loss in lung cancer cachexia mice by modulating AMPK pathways and regulating fatty acid β-oxidation.

### 2.6. The reprogramming of arginine metabolism contributes to the immunomodulatory effects of GLP in aged mice

Based on the above results, GLP was identified as a potential therapeutic agent for alleviating cancer cachexia. To further elucidate the molecular mechanisms through which GLP ameliorates cachexia, transcriptome sequencing was performed to compare the differentially expressed genes across three experimental conditions: untreated control, LLC-induced cachexia, and LLC-induced cachexia followed by GLP treatment. The results from KEGG pathway enrichment analysis revealed that differentially expressed genes were predominantly

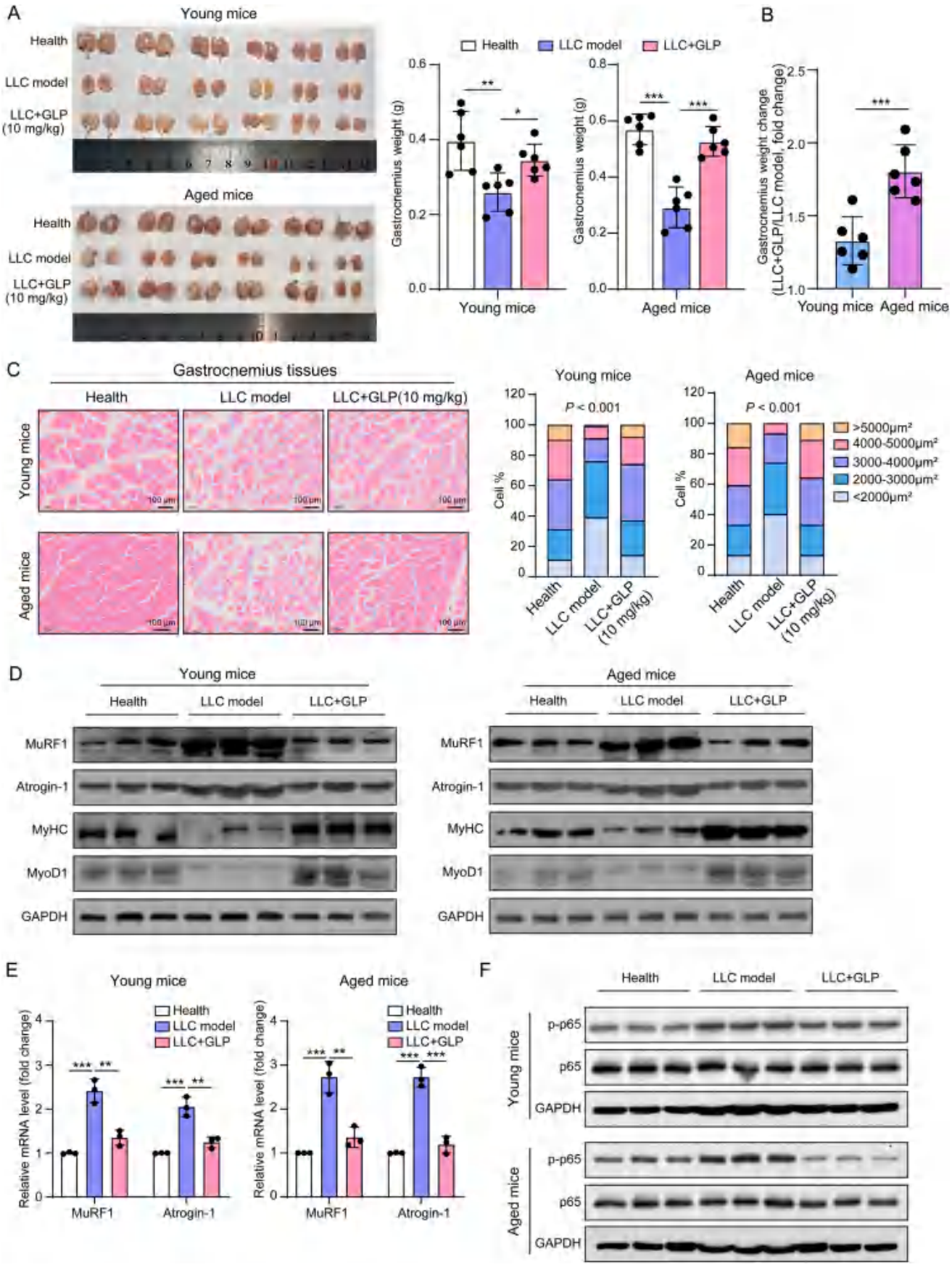


*(caption on next page)*

**Fig. 3.** Protective effects of GLP on myofiber atrophy in mice challenged with LLC tumors. (A) Representative images and corresponding weights of isolated GA muscles from health or LLC tumor-bearing mice, with or without GLP treatment (n = 6). (B) The GA weight change between young and aged mice. (C) Hematoxylin and eosin staining of GA muscle sections and quantitative analysis of myofiber cross-sectional area in the indicated groups; scale bar = 100 μm. (D) Representative Western blot showing protein expression of MuRF1, Atrogin-1, MyHC and MyoD1 in the GA tissues from health or LLC tumor-bearing mice, with or without GLP treatment. (E) qRT-PCR analysis of MuRF1 and Atrogin-1 mRNA levels in the GA tissues from health or LLC tumor-bearing mice in the presence or absence of GLP. (F) Western blot analysis of p-p65 and total p65 protein levels in GA tissues from health and LLC tumor-bearing mice with or without GLP treatment. Data are presented as mean ± SD. *, $P < 0.05$; **, $P < 0.01$; ***, $P < 0.001$.

enriched in the nitrogen metabolism pathway (Fig. 6A). Previous studies have demonstrated that arginine serves as a central node in nitrogen metabolism [25]. Therefore, arginine levels became the focus of our research. As shown in Fig. 6B, treatment with LLC or CT26 tumor supernatant indeed significantly reduced arginine levels in C2C12 cells compared to the healthy control group, whereas GLP treatment restored these levels. Additionally, in the mouse model, challenge of LLC tumors induced a reduction in serum arginine levels, which were subsequently converted to normal concentrations following GLP treatment (Fig. 6C). Low arginine conditions have been reported to help maintain the regulatory T cells (Treg) phenotype in $CD4^+$ T cells relying on oxidative metabolism and the ATF4-SLC7A11-GSH axis [26].

We next investigated whether GLP exerted enhanced therapeutic effects against tumor cachexia by modulating the function of $CD4^+$ T cells. Interesting to note that direct addition of arginine induced the formation of Tregs isolated from young group, as indicated by increased expression of CD25 and Foxp3, however, the effect of the same concentration was not significant in aged mice (Fig. 6D). Furthermore, by establishing the co-culture system and we noted that the CM from co-culture of LLC and C2C12 remarkably enhanced the percentage of Treg cells in young mice, but we didn't observe the similar phenotype in the aged mice (Fig. 6E–F). Notably, immunofluorescence staining demonstrated an increased number of Treg cells in the GA muscle of mice, whereas GLP treatment significantly reduced the number of Treg cells in these tumors (Fig. 6G). Importantly, GLP did not directly influence Treg differentiation (Supplementary Fig. S5A). This finding indicates that the recruitment of Treg during muscular inflammation facilitates tissue repair, explaining why aged groups exhibit compromised functional efficacy. Consequently, GLP demonstrates superior therapeutic efficacy in cohorts with geriatric cachexia.

## 3. Discussion

Lung cancer continues to be a significant global health issue, with both incidence and mortality rates on the rise. According to the Global Cancer Observatory, in 2020, there were approximately 2.2 million new cases of lung cancer, representing 11.4 % of all cancer diagnoses, and 1.79 million deaths, accounting for 18.0 % of total cancer-related fatalities [27]. Cancer cachexia, a complex metabolic syndrome characterized by progressive loss of skeletal muscle mass (with or without adipose tissue depletion) and refractory to conventional nutritional support, affects approximately one in five lung cancer patients [28]. With limited treatment options available, cachexia remains a significant challenge for these individuals. GLP, a bioactive polysaccharide derived from *Ganoderma lucidum*, has shown multiple therapeutic effects. Recent studies have shown that GLP exhibits promising effects in inhibiting cancer progression. Recent studies have demonstrated that crude GLP extracted from *G. lucidum* spores induced apoptosis in HCT116 colon cancer cells and inhibited tumor growth. This effect was attributed to the accumulation of autophagosomes and the suppression of autophagy flux, processes regulated by the MAPK/ERK signaling pathway [18]. In the present study, GLP, the principal active compound derived from the traditional Chinese medicine *Ganoderma lucidum*, demonstrated significant ameliorative effects on cancer cachexia both *in vitro* and *in vivo*. GLP not only relieves muscle atrophy by inactivating the NF-κB signaling pathway, but also suppresses lipolysis by modulating AMPK and fatty acid β-oxidation pathways. These findings suggest that GLP may be a promising candidate for the development of new therapeutic agents for cancer cachexia. AMPK is a central regulator of cellular energy homeostasis, and its activation under conditions of nutrient stress promotes lipid catabolism, thereby limiting lipid accumulation. Specifically, AMPK activation inhibits acetyl-CoA carboxylase (ACC), thereby reducing malonyl-CoA levels and fostering fatty acid mobilization from adipose tissue. Moreover, AMPK activation enhances the expression of enzymes involved in β-oxidation, such as carnitine palmitoyl transferase, which facilitates the transport of fatty acids into mitochondria for oxidation. This reduction in lipid storage and promotion of fatty acid oxidation is crucial in counteracting the lipid depletion seen in cancer cachexia.

Cumulative studies have shown that aging contributes to carcinogenesis and tumor progression, as well as increasing cancer-associated mortality [12,29]. In this study, by establishing a cancer cachexia model in aged mice, we found that the symptoms of cachexia were more pronounced in older mice, manifesting as greater losses in body weight, skeletal muscle, and adipose tissue. These complex interactions indicate that inflammatory factors in the tumor microenvironment are significantly associated with age-related cancer cachexia. Consequently, targeting these inflammatory pathways may provide a potential therapeutic strategy to alleviate cachexia in lung cancer by intervening in the aging process [30,31]. Interestingly, our results indicated that GLP resulted in better remission of cachexia in aged mice, suggesting that GLP may alleviate cancer cachexia through anti-aging mechanisms. We provide important evidence linking aging and cancer cachexia. Further investigations are warranted to elucidate the mechanisms by which the anti-aging effects of GLP contribute to alleviating cancer cachexia.

Cancer cachexia is now recognized not merely as a systemic metabolic complication but as a process intensely orchestrated by the dynamic and multifaceted tumor microenvironment (TME). Within this milieu, a complex interplay of inflammatory mediators and cellular crosstalk drives the profound metabolic alterations characteristic of cachexia [32]. A critical crosstalk has been reported in pancreatic cancer cachexia, where CCL2-mediated recruitment of macrophages by tumor cells activates a TWEAK-dependent signaling axis that promotes muscle wasting [33]. This finding uncovers that the tumor immune microenvironment plays an important role in cancer progression and cachexia. Wang et al. demonstrated that a homogeneous GLP isolated from *Ganoderma lucidum* fruiting bodies enhances antitumor immunity by regulating immune cell differentiation and inhibiting the accumulation of myeloid-derived suppressor cells (MDSCs) in both spleen and tumor tissues. This immune-modulating effect is mediated through the CARD9-NF-κB signaling pathway, suggesting a mechanism by which GLP can alleviate immune suppression within the tumor microenvironment [34]. Interesting to note that Tregs are now recognized as a central driver of cancer cachexia. Tregs play a modulatory role in skeletal muscle repair [35]. Additionally, Tregs in epididymal visceral adipose tissue are important to maintaining adipose tissue and metabolic homeostasis. Although GLP is known to regulate immune function, its specific mechanisms remain unclear. This study elucidates that GLP exerts immunomodulatory effects by reprogramming of arginine metabolism. In younger populations, $CD4^+$ T cells exhibit heightened sensitivity to arginine metabolic reprogramming, effectively inducing functional Treg generation to mitigate cachexia-associated skeletal muscle deterioration. Conversely, aged groups demonstrate diminished metabolic adaptability, failing to establish adequate functional Treg populations. This age-associated immune metabolic deficiency enhances

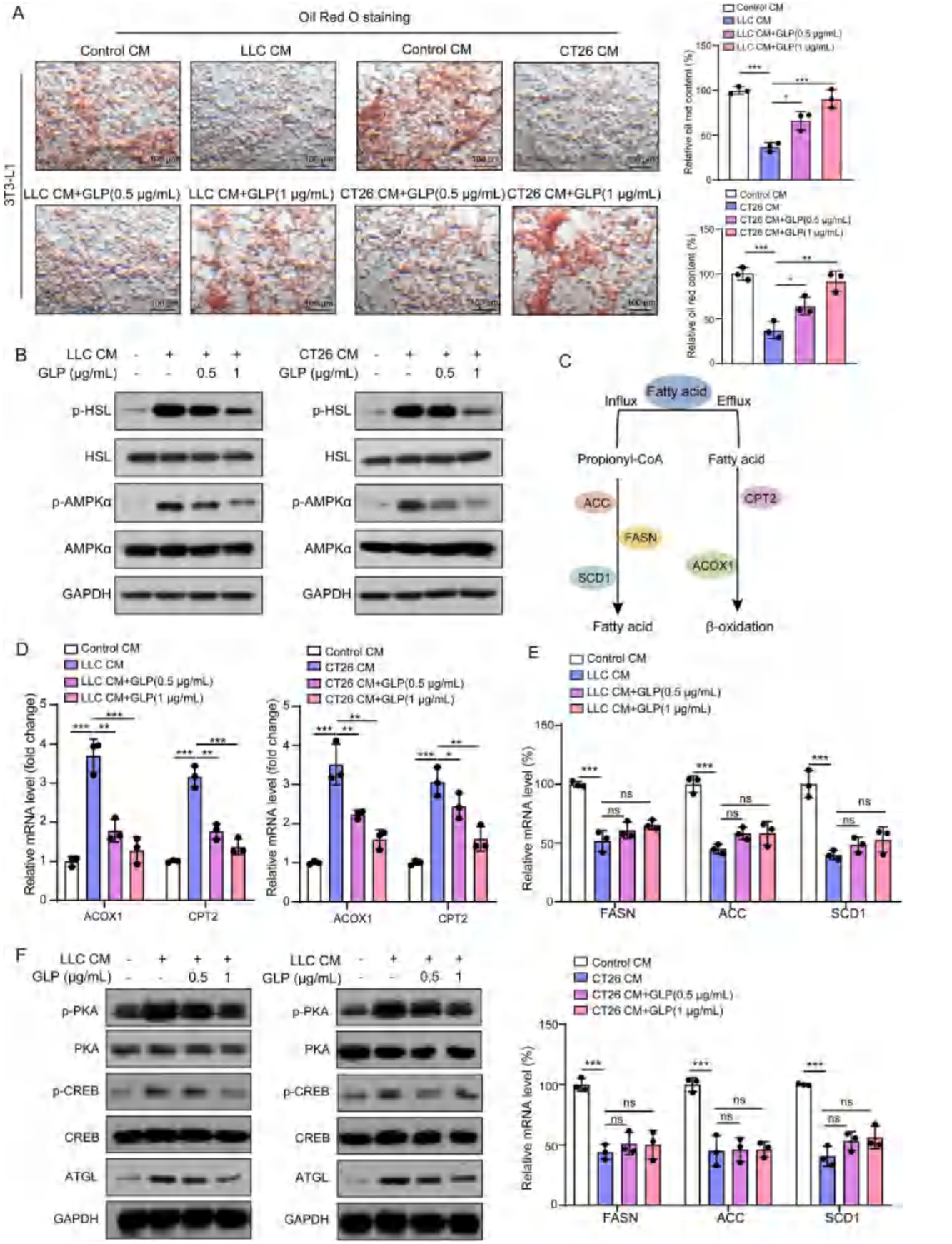


*(caption on next page)*

**Fig. 4.** Impact of GLP on lipolysis in 3T3-L1 adipocytes *in vitro*. (A) Representative images of Oil Red O staining showing lipid droplet content in 3T3-L1 adipocytes treated with LLC or CT26-derived CM, with or without GLP; scale bar = 100 μm. (B) Western blot analysis of phosphorylated HSL (p-HSL), total HSL, phosphorylated AMPKα (p-AMPKα), and total AMPKα protein levels in 3T3-L1 adipocytes treated with LLC or CT26-derived CM in the presence or absence of GLP. (C) The diagram showing fatty acid synthesis and β-oxidation. (D and E) qRT-PCR quantification of mRNA expression levels of lipogenesis and fatty acid β-oxidation related genes, including FASN, ACC, ASCL1, ACOX1, and CPT2, in 3T3-L1 adipocytes treated with LLC or CT26-derived CM, with or without GLP. (F) Western blot analysis of phosphorylated PKA (p-PKA), total PKA, phosphorylated CREB (p-CREB), total CREB and ATGL protein levels in 3T3-L1 adipocytes treated with LLC or CT26-derived CM in the presence or absence of GLP. Data are presented as mean ± SD. *, $P < 0.05$; **, $P < 0.01$; ***, $P < 0.001$; ns, no significant difference.

the therapeutic efficacy of GLP in elderly cohorts. GLP significantly alleviates cachexia progression caused by Treg insufficiency.

In summary, the results of this study provide the first evidence that GLP can effectively attenuate cancer cachexia, by exerting significant bioactivity in alleviating skeletal muscle atrophy, reducing lipolysis, and exhibiting immunomodulatory effects through the reprogramming of arginine metabolism, with minimal toxicity to both cells and animals (Fig. 7). These findings suggest that GLP may be a promising strategy in the management of cancer cachexia.

## 4. Materials and methods

### 4.1. Cell culture

Lewis lung cancer cell line (LLC) was obtained from the National Collection of Authenticated Cell Cultures (Shanghai, China), and maintained in DMEM medium (Thermo Fisher Scientific, Waltham, MA, USA) supplemented with 10 % FBS (ExCell Bio, Shanghai, China) at 37 °C, 5 % $CO_2$. CT26 colon carcinoma cells, obtained from the American Type Culture Collection (ATCC), were cultured in RPMI 1640 medium (Thermo Fisher Scientific) supplemented with 10 % FBS at 37 °C in a 5 % $CO_2$ atmosphere. The C2C12 murine myoblast cell line and the 3T3-L1 pre-adipocyte cell line, both acquired from ATCC, were cultured in DMEM supplemented with 10 % FBS at 37 °C in a 5 % CO2 atmosphere. For C2C12 cell differentiation, cells were maintained in DMEM containing 2 % horse serum until they reached 70 % confluence, and were then induced to differentiate for 5–8 days. For 3T3-L1 cell differentiation, upon reaching 100 % confluence for 48 h in standard culture medium, the medium was replaced with DMEM containing 10 % FBS, 10 μg/mL insulin (Beyotime, Shanghai, China), 1 μM dexamethasone (Beyotime), and 0.5 mM 3-isobutyl-1-methylxanthine (Beyotime), and the cells were induced to differentiate for 48 h.

### 4.2. Source and extraction of crude *Ganoderma lucidum* polysaccharide

GLP was provided by GuangZhou Shan Yuan Tang Health Science and Technology Co., LTD (Guangzhou, P.R. China). The production process for *Ganoderma lucidum* polysaccharides follow a structured sequence of steps. First, *Ganoderma lucidum* is extracted with water (8 times its weight) in two 1.5-h sessions. The mixtures are filtered and combined into one solution. Next, the solution is concentrated under vacuum at 70–80 °C and 0.08 MPa, then dried at 60–70 °C to form a solid. Finally, the solid is pulverized and sifted through an 80-mesh screen to produce the final crude *Ganoderma lucidum* polysaccharide. The components of crude *Ganoderma lucidum* polysaccharides are shown in Supporting Information Table S3.

### 4.3. Oil Red O staining

Oil Red O staining was performed to assess lipolysis in 3T3-L1 cells using the Oil Red O Staining Kit (Beyotime) following the manufacturer's instructions. Briefly, cells were fixed with 4 % formaldehyde for 10 min and rinsed twice with PBS. The cells were stained with Oil Red O solution for 15 min. After rinsing with PBS, the cells were examined and imaged under a microscope.

### 4.4. Senescence β-galactosidase staining

Cellular senescence was detected using a senescence β-galactosidase staining kit (Beyotime). The adherent cells were incubated with fixative buffer for 15 min and stained with a working staining solution containing β-galactosidase substrate at 37 °C for 16 h. Cells were visualized under a bright-field microscope, and the percentage of cells positively stained was calculated.

### 4.5. Western blot analysis

Western blot experiments were performed as previously described [36]. Protein concentration was measured using the Pierce BCA Protein Assay Kit (Thermo Fisher Scientific). Equal amounts of protein samples were separated by SDS-PAGE and transferred onto PVDF membranes (Bio-Rad, Hercules, USA). After blocking with non-fat milk, the membrane was incubated overnight at 4 °C with primary antibodies and then with corresponding secondary antibodies for 1 h. The membrane was washed with TBST for 30 min, and the signal was detected using an ECL substrate (Bio-Rad).

### 4.6. qRT-PCR

The process used for quantitative real-time polymerase chain reaction (qRT–PCR) has been described elsewhere [37]. Total RNA was extracted using the Hipure Total RNA Kit (Magen Biotechnology, Guangzhou, China), and reverse transcription was then carried out to synthesize cDNA using the PrimeScript™ RT Reagent Kit with gDNA Eraser. Quantitative PCR (qPCR) was performed using the SYBR Green qPCR SuperMix (Transgene, Beijing, China) on a CFX96 Touch Real-Time PCR Detection System (Bio-Rad). The relative mRNA expression of target genes was normalized to that of actin. The RT-qPCR primer sequences are listed in Supporting Information in Table S1.

### 4.7. RNA sequencing (RNA-seq)

Total RNA was isolated from C2C12 cells using TRIzol reagent (Invitrogen, CA, USA), and mRNA was subsequently enriched with Oligo (dT) beads. The enriched RNA was fragmented, reverse transcribed using random hexamer (N6) primers, and then converted into double-stranded cDNA. Following end repair, addition of an “A" tail, and adapter ligation, the resulting fragments were amplified by PCR. The amplified products were circularized and subjected to sequencing using the DNBSEQ platform (PE150). After quality control (QC), clean reads were aligned to the reference genome, and mapping rates as well as read distribution were assessed. Data passing QC were used for gene quantification, expression analyses, and functional enrichment. The differentially expressed genes (Supporting Information Table S2) were subsequently analyzed for KEGG pathway enrichment.

### 4.8. Arginine measurements

Arginine levels in culture supernatants and mouse serum were measured using a commercial Arginine ELISA kit (Abebio Science, Wuhan, China) according to the manufacturer's instructions.

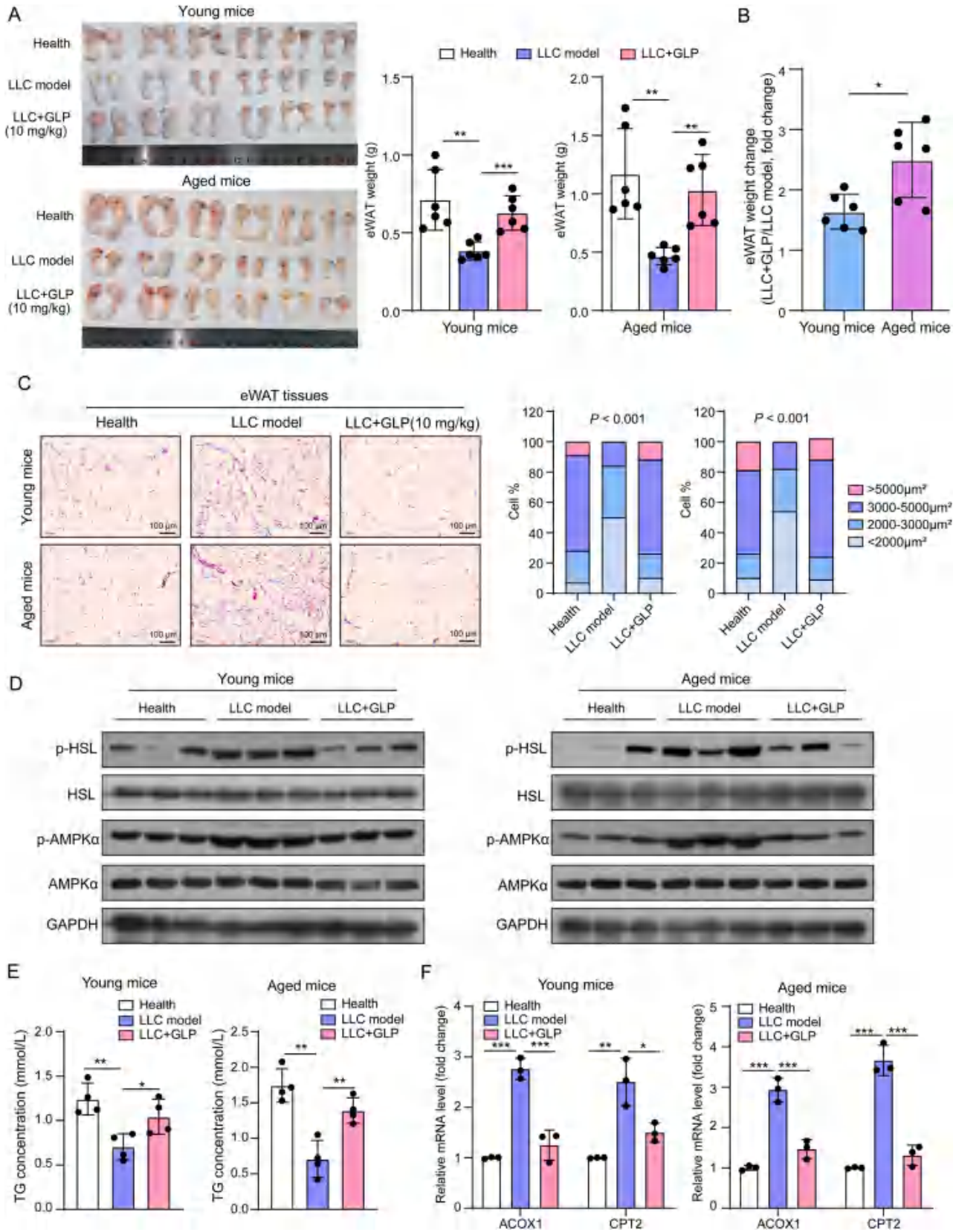


**Fig. 5.** GLP enhances eWAT homeostasis in mice through the modulation of AMPK signaling and fatty acid β-**oxidation.** (A) Representative images and corresponding weights of eWAT isolated from health, LLC tumor-bearing mice with or without treatment of GLP (n = 6). (B) The eWAT weight change between young and aged mice. (C) Histological examination of eWAT by H&E staining and morphometric analysis of adipocyte cross-sectional area in eWAT sections; scale bar = 100 μm. (D) Western blot analysis of p-HSL, total HSL, p-AMPKα, and total AMPKα protein levels in eWAT from health and LLC tumor-bearing mice with or without GLP administration. (E) Content of TG in serum with or without treatment of GLP. (F) qRT-PCR analysis of ACOX1 and CPT2 mRNA levels in the eWAT from mice as presented groups. Data are presented as mean ± SD. *, $P < 0.05$; **, $P < 0.01$; ***, $P < 0.001$.

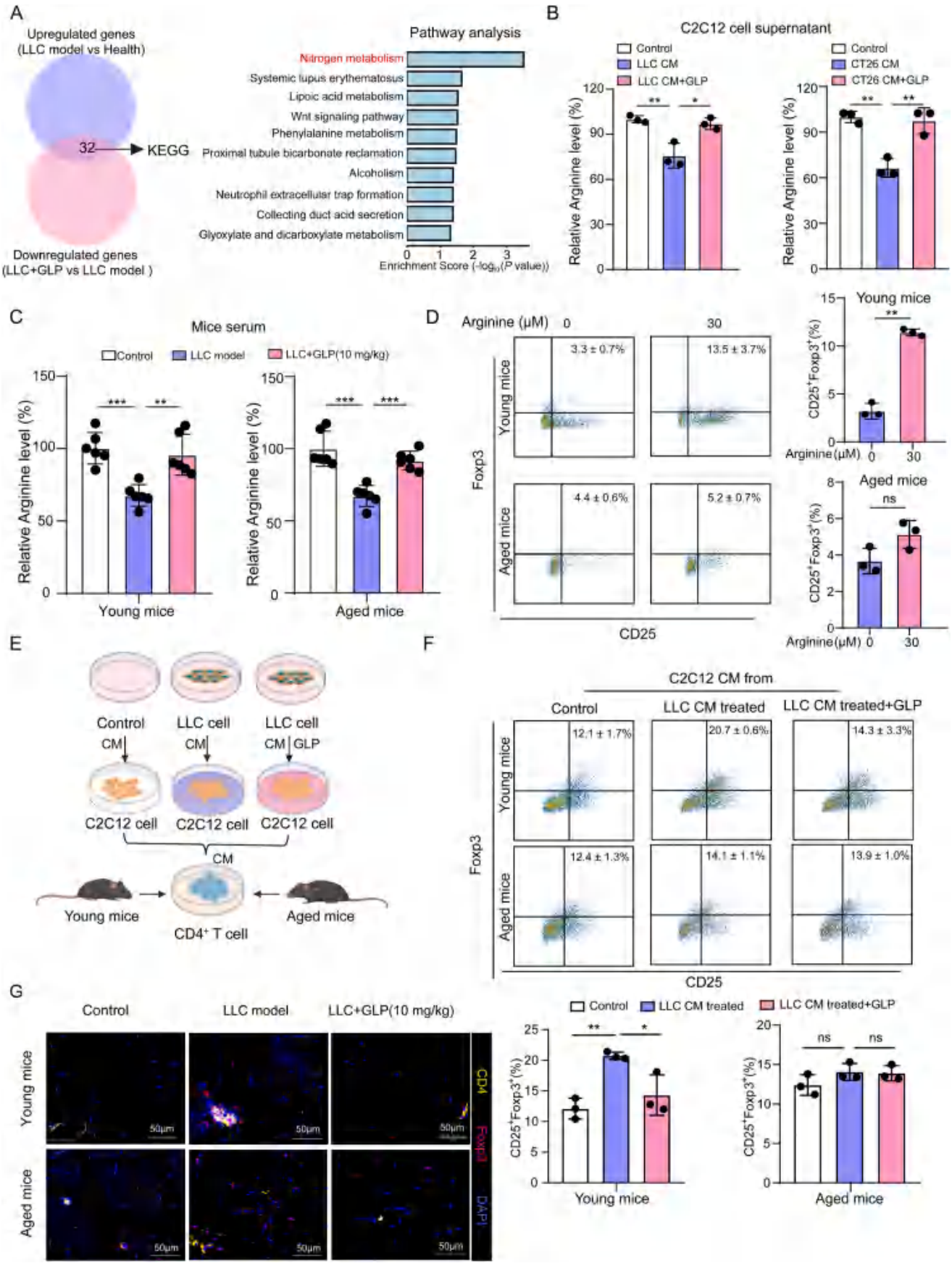


*(caption on next page)*

**Fig. 6.** GLP exhibits immunomodulatory effects and demonstrates a favorable safety profile in LLC tumor-bearing mice. (A) KEGG pathway enrichment analysis was performed on differentially expressed genes identified in C2C12 cells across three experimental conditions: untreated control, LLC-induced, and LLC-induced followed by GLP treatment. (B) Arginine concentrations in the supernatant of C2C12 cells under various treatment conditions were quantified using ELISA. (C) Serum arginine concentrations were quantified by ELISA in different experimental groups of mice (n = 6). (D) Flow cytometric analysis was performed to determine the percentage of Treg (defined as $CD25^{+}Foxp3^{+}$) in $CD4^{+}$ T cells exposed to differentially conditioned media from C2C12 cells. (E) The diagram showing the establishment of co-culture system. (F) The percentage of Treg cells among groups as indicated. (G) Representative images show simultaneous detection of CD4 and Foxp3 in GA muscle sections. Nuclei were counterstained with DAPI (blue). Scale bar: 50 μm. Data are presented as mean ± SD. *, $P < 0.05$; **, $P < 0.01$; ***, $P < 0.001$.

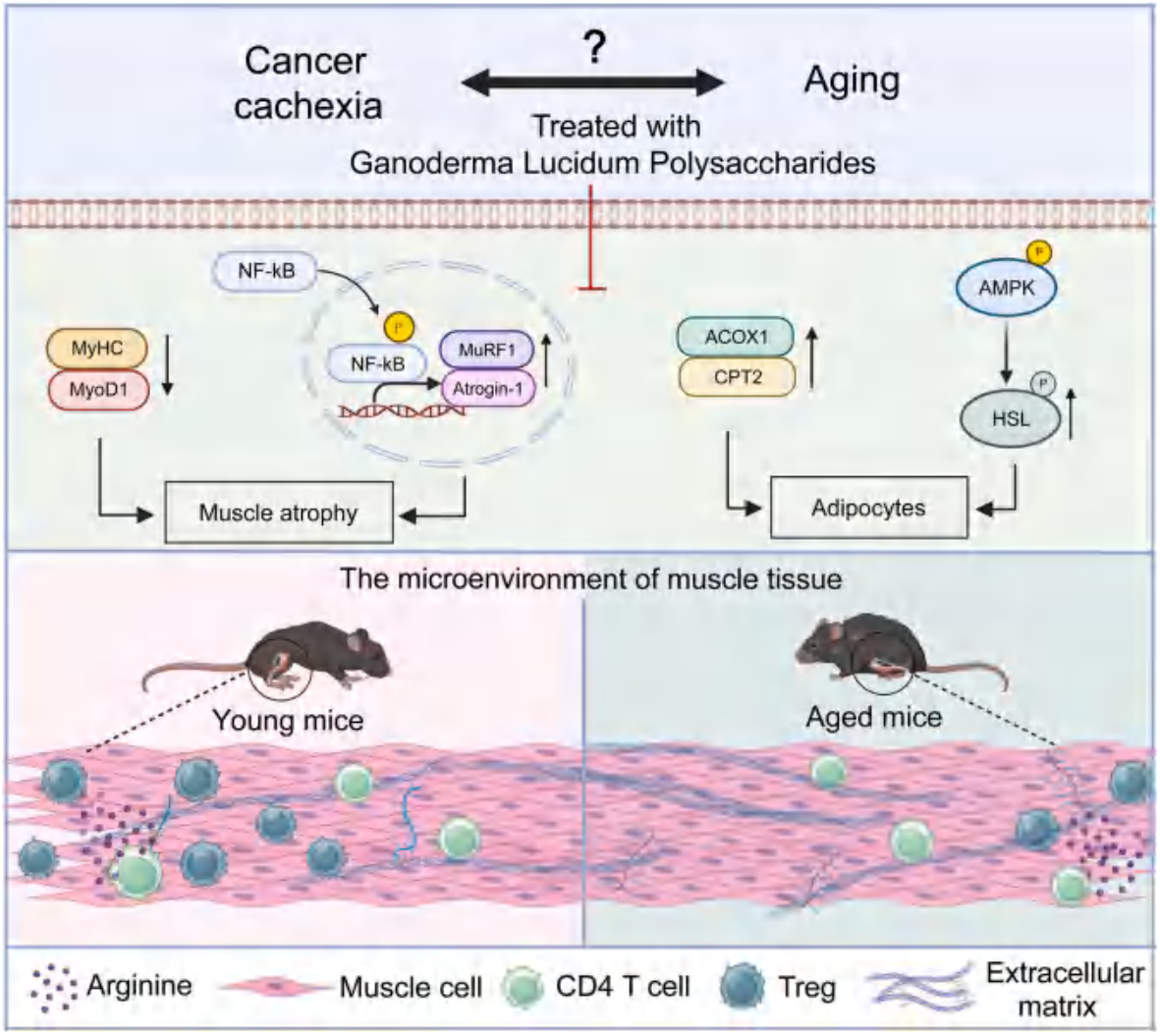


**Fig. 7.** Schematic diagram summarizing how GLP attenuates cancer cachexia.

### 4.9. Mouse $CD4^{+}$ T cell isolation and co-culture

$CD4^{+}$ T cells were isolated from mouse spleens using a $CD4^{+}$ T Cell Isolation Kit (Miltenyi Biotec, Germany) through magnetic-activated cell sorting (MACS). Briefly, splenocytes were dissociated and labeled with a biotin-conjugated antibody cocktail targeting non-$CD4^{+}$ cells, followed by anti-biotin microbeads. The $CD4^{+}$ T cell-enriched fraction was obtained by negative selection. The isolated cells were cultured in RPMI-1640 medium supplemented with 10 % FBS, 1 % penicillin-streptomycin, 2 mM L-glutamine, 50 μM β-mercaptoethanol, and 10 ng/mL IL-2. For activation, cells were stimulated with plate-bound anti-CD3 (5 μg/mL) and soluble anti-CD28 (2 μg/mL) antibodies. The cells were maintained at 37 °C in a 5 % $CO_2$ atmosphere and passaged as needed. For co-culture, $CD4^{+}$ T cells were treated with different conditioned medium (CM) from LLC cells or colorectal adenocarcinoma cells (CT26) for 5–7 days. Subsequent analyses included flow cytometry for Treg cell markers.

### 4.10. Flow cytometric analysis

Flow cytometry samples were acquired on a BD FACSAria II and analyzed using FlowJo software. Live cells were identified using the LIVE/DEAD Fixable Aqua Dead Cell Stain (Thermo Fisher Scientific). Following surface marker staining, cells were fixed and permeabilized using the Foxp3/Transcription Factor Fixation/Permeabilization buffer set (Thermo Fisher Scientific) for subsequent intracellular staining with specific antibodies.

### 4.11. Multiplex immunohistochemistry (mIHC)

For multiplex staining, sequential rounds of immunolabeling were performed with primary antibodies against target proteins (CD4 and

Foxp3), followed by horseradish peroxidase (HRP)-conjugated secondary antibodies and tyramide signal amplification (TSA) using fluorophores. After each round, antibodies were stripped via heat-induced epitope retrieval to prevent cross-reactivity. Nuclei were counterstained with DAPI. Slides were imaged using a multispectral fluorescence microscope, and spectral unmixing was performed to resolve overlapping signals.

### 4.12. Animals

Male C57BL/6 mice, aged either 4 or 18 months, were obtained from Shanghai MODEL Organism (Shanghai, China). All animal experiments were approved by the Ethics Committee for Animal Experiments at Guangzhou Medical University and were maintained under standard conditions in accordance with institutional guidelines.

### 4.13. Cancer cachexia model in vivo

Male C57BL/6 mice of the same age were randomly assigned to three groups (6 mice per group): a healthy control group, an LLC tumor-bearing group, and an LLC tumor-bearing group treated with 10 mg/kg GLP. Mice were subcutaneously implanted in the right flank with $5 \times 10^5$ of (100 μL) LLC cells on day 0. Starting from day 8, mice in the LLC model group were gavaged with sterile saline, while GLP-treated mice received GLP (10 mg/kg) every two days. Body weight, tumor volume, and food intake were measured for each group every two days from day 8 until the conclusion of the experiment. The longest diameter (L) and shortest diameter (W) of each tumor were recorded using a vernier calliper. The tumor volume was calculated using the formula: $V = 0.5 \times L \times W^2$. At the end of the experiment, all animals were euthanized through anesthesia. The GA muscles and eWAT were rapidly dissected, weighed, frozen in liquid nitrogen, and stored at −80 °C until further analysis, or fixed in 4 % paraformaldehyde overnight before being embedded in paraffin.

### 4.14. Hematoxylin-Eosin staining

Hematoxylin-Eosin staining was performed as described previously [38]. GA and eWAT tissue embedded in paraffin were cut into 5 μm sections and then stained with H&E by standard procedures. Briefly, tissue sections were dewaxed using xylene, stained with hematoxylin for 2 min, differentiated with hydrochloric acid alcohol for 10 s, washed with water for 3 min, and stained with eosin for 30 s. The staining was visualized under bright-field microscopy.

### 4.15. Blood chemistry analysis

Peripheral blood was collected into anticoagulant tubes after the mouse were anesthetized. The quantities and percentages of WBCs, RBCs, HGB, PLTs, neutrophils, and lymphocytes in the blood were assessed using a hematology analyser (Mindray, Wuhan, China). Serum levels of ALT, AST, and triglycerides were determined using specific assay kits.

### 4.16. Statistical analysis

The data were presented as mean ± SD and compared using the Student's t-test. *P*-values less than 0.05 were considered statistically significant in all experiments. All statistical analyses were performed using GraphPad Prism 8.0. *P*-values were presented as $^*P < 0.05$, $^{**}P < 0.01$, $^{***}P < 0.001$.

Clinical data of 40 patients with cancer cachexia were obtained from a previously published study [20]. Patients were stratified into two age groups (<65 years and ≥65 years). Body weight loss over the past 6 months was compared between the two groups. The data were assessed using the Wilcoxon rank-sum test, a non-parametric method that evaluates whether two independent samples originate from the same distribution by comparing their rank sums.

## CRediT authorship contribution statement

**Chunmiao Deng:** Writing – original draft, Visualization, Validation, Data curation. **Yunfang Chen:** Writing – review & editing, Visualization, Validation, Resources, Funding acquisition. **Jiaojiao Xu:** Writing – original draft, Visualization, Validation, Data curation. **Chanjin Liang:** Writing – original draft, Software, Methodology, Investigation. **Cui Shao:** Writing – original draft, Software, Methodology, Investigation. **Shiqi Mei:** Writing – original draft, Software, Methodology, Investigation. **Yongkang Xu:** Validation, Methodology. **Yin Li:** Writing – original draft, Software, Methodology, Investigation. **Cancan Zheng:** Writing – review & editing, Supervision, Resources, Funding acquisition, Conceptualization. **Yichang Luo:** Writing – review & editing, Supervision, Resources, Funding acquisition, Conceptualization. **Xingyuan Shi:** Writing – review & editing, Supervision, Resources, Funding acquisition, Conceptualization.

## Ethics approval and consent to participate

The animal experiments were approved by the Ethics Committee for Animal Experiments of Guangzhou Medical University. All procedures were performed in strict compliance with the ARRIVE guidelines and institutional ethical standards for animal welfare.

## Declaration of competing interest

The authors declare no conflict of interest.

## Acknowledgements

This study was supported by National Natural Science Foundation of China (82204455, 32470804), Guangdong Natural Science Research International joint project (2025A1515010195), the Science and Technology Program of Guangzhou (2025A03J3287, 2025A04J3563), Guangzhou Science and Technology Fund (2024A03J0786, 2024A03J0784), the Guangzhou Major Medical Disciplines Project (2025–2027), 2023 Guangdong Provincial Clinical Key Specialty Construction Project (2022-39) and the Wu Jieping Medical Foundation (320.6750.2023-5-110).

## Appendix A. Supplementary data

Supplementary data to this article can be found online at https://doi.org/10.1016/j.canlet.2026.218247.

## Data availability

The RNA-seq data generated in this study are publicly available in the Genome Sequence Archive (GSA) at CRA035989. The data supporting the findings of this study are available within the article. Additional data related to this research may be requested from the corresponding authors upon reasonable request.

## References

[1] E. Morgan, I. Soerjomataram, H. Rumgay, H.G. Coleman, A.P. Thrift, J. Vignat, M. Laversanne, J. Ferlay, M. Arnold, The global landscape of esophageal squamous cell carcinoma and esophageal adenocarcinoma incidence and mortality in 2020 and projections to 2040: new estimates from GLOBOCAN 2020, Gastroenterology 163 (2022) 649–658 e642.

[2] O. Al-Sawaf, J. Weiss, M. Skrzypski, J.M. Lam, T. Karasaki, F. Zambrana, A.C. Kidd, A.M. Frankell, T.B.K. Watkins, C. Martinez-Ruiz, C. Puttick, J.R.M. Black, A. Huebner, M.A. Bakir, M. Sokac, S. Collins, S. Veeriah, N. Magno, C. Naceur-Lombardelli, P. Prymas, A. Toncheva, S. Ward, N. Jayanth, R. Salgado, C.P. Bridge, D.C. Christiani, R.H. Mak, C. Bay, M. Rosenthal, N. Sattar, P. Welsh, Y. Liu,

N. Perrimon, K. Popuri, M.F. Beg, N. McGranahan, A. Hackshaw, D.M. Breen, S. O'Rahilly, N.J. Birkbak, H. Aerts, T.R. Consortium, M. Jamal-Hanjani, C. Swanton, Body composition and lung cancer-associated cachexia in TRACERx, Nat. Med. 29 (2023) 846–858.
[3] V.E. Baracos, L. Martin, M. Korc, D.C. Guttridge, K.C.H. Fearon, Cancer-associated cachexia, Nat. Rev. Dis. Primers 4 (2018) 17105.
[4] A. Du, Z. Wang, T. Huang, S. Xue, C. Jiang, G. Qiu, K.J.M.O. Yuan, Fatty Acids in Cancer: Metabolic Functions and Potential Treatment, 2, 2023, p. e25.
[5] J.M. Argiles, F.J. Lopez-Soriano, B. Stemmler, S. Busquets, Cancer-associated cachexia - understanding the tumour macroenvironment and microenvironment to improve management, Nat. Rev. Clin. Oncol. 20 (2023) 250–264.
[6] A. Maccio, E. Sanna, M. Neri, S. Oppi, C. Madeddu, Cachexia as evidence of the mechanisms of resistance and tolerance during the evolution of cancer disease, Int. J. Mol. Sci. 22 (2021).
[7] C. Madeddu, S. Busquets, C. Donisi, E. Lai, A. Pretta, F.J. Lopez-Soriano, J. M. Argiles, M. Scartozzi, A. Maccio, Effect of cancer-related cachexia and associated changes in nutritional status, inflammatory status, and muscle mass on immunotherapy efficacy and survival in patients with advanced non-small cell lung cancer, Cancers (Basel) 15 (2023).
[8] P. Jin, X.D. Feng, C.S. Huang, J. Li, H. Wang, X.M. Wang, L. Li, L.Q.J.M.O. Ma, Oxidative Stress and Cellular Senescence: Roles in Tumor Progression and Therapeutic Opportunities, 3, 2024 e70007.
[9] F. Penna, G. Rubini, P.J. Costelli, Immunomodulation: a new approach to cancer cachexia, potentially suitable for, Aging 100 (2024) 101318.
[10] T. Wang, D. Zhou, Z. Hong, Sarcopenia and cachexia: molecular mechanisms and therapeutic interventions, MedComm 6 (2025) e70030.
[11] S. Haston, E. Gonzalez-Gualda, S. Morsli, J. Ge, V. Reen, A. Calderwood, I. Moutsopoulos, L. Panousopoulos, P. Deletic, G. Carreno, R. Guiho, S. Manshaei, J.M. Gonzalez-Meljem, H.Y. Lim, D.J. Simpson, J. Birch, H.A. Pallikonda, T. Chandra, D. Macias, G.J. Doherty, D.M. Rassl, R.C. Rintoul, M. Signore, I. Mohorianu, A.N. Akbar, J. Gil, D. Munoz-Espin, J.P. Martinez-Barbera, Clearance of senescent macrophages ameliorates tumorigenesis in KRAS-driven lung cancer, Cancer Cell 41 (2023) 1242–1260 e1246.
[12] L. Montegut, C. Lopez-Otin, G. Kroemer, Aging and cancer, Mol. Cancer 23 (2024) 106.
[13] Z. Hu, W. Lei, W.J.M.O. Wen, Comprehensive Analysis of cuproptosis-related Gene Expression and Positive Correlations with CD4+ T Cell Infiltration in Head and Neck Squamous Cell Carcinoma, 2, 2023, p. e42.
[14] E. Seweryn, A. Ziala, A. Gamian, Health-promoting of polysaccharides extracted from Ganoderma lucidum, Nutrients 13 (2021).
[15] Z.B. Lin, Cellular and molecular mechanisms of immuno-modulation by Ganoderma lucidum, J. Pharmacol. Sci. 99 (2005) 144–153.
[16] Y. Kan, T. Chen, Y. Wu, J. Wu, J. Wu, Antioxidant activity of polysaccharide extracted from Ganoderma lucidum using response surface methodology, Int. J. Biol. Macromol. 72 (2015) 151–157.
[17] K. Zhang, Y. Liu, X. Zhao, Q. Tang, J. Dernedde, J. Zhang, H. Fan, Anti-inflammatory properties of GLPss58, a sulfated polysaccharide from Ganoderma lucidum, Int. J. Biol. Macromol. 107 (2018) 486–493.
[18] C. Guo, D. Guo, L. Fang, T. Sang, J. Wu, C. Guo, Y. Wang, Y. Wang, C. Chen, J. Chen, R. Chen, X. Wang, Ganoderma lucidum polysaccharide modulates gut microbiota and immune cell function to inhibit inflammation and tumorigenesis in colon, Carbohydr. Polym. 267 (2021) 118231.
[19] H.S. Chen, Y.F. Tsai, S. Lin, C.C. Lin, K.H. Khoo, C.H. Lin, C.H. Wong, Studies on the immuno-modulating and anti-tumor activities of Ganoderma lucidum (Reishi) polysaccharides, Bioorg. Med. Chem. 12 (2004) 5595–5601.
[20] Q.J. Yang, J.R. Zhao, J. Hao, B. Li, Y. Huo, Y.L. Han, L.L. Wan, J. Li, J. Huang, J.J.J. o.c. Lu, Sarcopenia, Muscle, Serum and Urine Metabolomics Study Reveals a Distinct Diagnostic Model for Cancer Cachexia, 9, 2018, pp. 71–85.
[21] L.F. Zheng, P.J. Chen, W.H. Xiao, [Signaling pathways controlling skeletal muscle mass], Sheng Li Xue Bao 71 (2019) 671–679.
[22] A. Ito, M. Hashimoto, J. Tanihata, S. Matsubayashi, R. Sasaki, S. Fujimoto, H. Kawamoto, Y. Hosaka, A. Ichikawa, T. Kadota, Y. Fujita, D. Takekoshi, S. Ito, S. Minagawa, T. Numata, H. Hara, T. Matsuoka, J. Udaka, J. Araya, M. Saito, K. Kuwano, Involvement of Parkin-mediated mitophagy in the pathogenesis of chronic obstructive pulmonary disease-related sarcopenia, J Cachexia Sarcopenia Muscle 13 (2022) 1864–1882.
[23] J. von Renesse, P. Mirtschink, Ectodysplasin A2 receptor-NF-kappaB-inducing kinase axis: a new player in muscle wasting to cancer cachexia, Signal Transduct. Targeted Ther. 8 (2023) 383.
[24] S. Lu, Y. Li, Q. Shen, W. Zhang, X. Gu, M. Ma, Y. Li, L. Zhang, X. Liu, X. Zhang, Carnosol and its analogues attenuate muscle atrophy and fat lipolysis induced by cancer cachexia, J Cachexia Sarcopenia Muscle 12 (2021) 779–795.
[25] T.S. Fung, K.W. Ryu, C.B. Thompson, Arginine: at the crossroads of nitrogen metabolism, EMBO J. 44 (2025) 1275–1293.
[26] Z. Zou, Q. Cheng, J. Zhou, C. Guo, A.V. Hadjinicolaou, M. Salio, X. Liang, C. Yang, Y. Du, W. Yao, D. Wang, V. Cerundolo, Q. Wang, M. Xia, ATF4-SLC7A11-GSH axis mediates the acquisition of immunosuppressive properties by activated CD4(+) T cells in low arginine condition, Cell Rep. 43 (2024) 113995.
[27] H. Sung, J. Ferlay, R.L. Siegel, M. Laversanne, I. Soerjomataram, A. Jemal, F. Bray, Global cancer statistics 2020: GLOBOCAN estimates of incidence and mortality worldwide for 36 cancers in 185 countries, CA Cancer J. Clin. 71 (2021) 209–249.
[28] T. Shukuya, K. Takahashi, Y. Shintani, K. Miura, I. Sekine, K. Takayama, A. Inoue, I. Okamoto, K. Kiura, T. Kawaguchi, N. Yamamoto, E. Miyaoka, I. Yoshino, H. Date, Epidemiology, risk factors and impact of cachexia on patient outcome: results from the Japanese lung cancer registry study, J Cachexia Sarcopenia Muscle 14 (2023) 1274–1285.
[29] V. Boccardi, L. Marano, Aging, cancer, and inflammation: the telomerase connection, Int. J. Mol. Sci. 25 (2024).
[30] A. Ozdemir, Y.D. Simay Demir, Z.E. Yesilyurt, M. Ark, Senescent cells and SASP in cancer microenvironment: new approaches in cancer therapy, Adv. Protein Chem. Struct. Biol. 133 (2023) 115–158.
[31] S.K. Jha, G. De Rubis, S.R. Devkota, Y. Zhang, R. Adhikari, L.A. Jha, K. Bhattacharya, S. Mehndiratta, G. Gupta, S.K. Singh, N. Panth, K. Dua, P. M. Hansbro, K.R. Paudel, Cellular senescence in lung cancer: molecular mechanisms and therapeutic interventions, Ageing Res. Rev. 97 (2024) 102315.
[32] A.N. Hosein, R.A. Brekken, A. Maitra, Pancreatic cancer stroma: an update on therapeutic targeting strategies, nature reviews, Gastroenterol. Hepatol. 17 (2020) 487–505.
[33] M. Liu, Y. Ren, Z. Zhou, J. Yang, X. Shi, Y. Cai, A.X. Arreola, W. Luo, K.M. Fung, C. Xu, R.D. Nipp, M.S. Bronze, L. Zheng, Y.P. Li, C.W. Houchen, Y. Zhang, M. Li, The crosstalk between macrophages and cancer cells potentiates pancreatic cancer cachexia, Cancer Cell 42 (2024) 885–903.e884.
[34] Y. Wang, X. Fan, X. Wu, Ganoderma lucidum polysaccharide (GLP) enhances antitumor immune response by regulating differentiation and inhibition of MDSCs via a CARD9-NF-κB-IDO pathway, Biosci. Rep. 40 (2020).
[35] J. Wu, B. Ren, D. Wang, H.J.C.d. Lin, Disease, Regulatory T Cells in Skeletal Muscle Repair and Regeneration: Recent Insights, 13, 2022, p. 680.
[36] C. Zheng, X. Yu, T. Xu, Z. Liu, Z. Jiang, J. Xu, J. Yang, G. Zhang, Y. He, H. Yang, X. Shi, Z. Li, J. Liu, W.W. Xu, KCTD4 interacts with CLIC1 to disrupt calcium homeostasis and promote metastasis in esophageal cancer, Acta Pharm. Sin. B 13 (2023) 4217–4233.
[37] C.C. Zheng, L. Liao, Y.P. Liu, Y.M. Yang, Y. He, G.G. Zhang, S.J. Li, T. Liu, W.W. Xu, B. Li, Blockade of nuclear β-Catenin signaling via direct targeting of RanBP3 with NU2058 induces cell senescence to suppress colorectal tumorigenesis, Adv. sci. (Weinheim, Baden-Wurttemberg, Germany) 9 (2022) e2202528.
[38] C. Zheng, X. Yu, Y. Liang, Y. Zhu, Y. He, L. Liao, D. Wang, Y. Yang, X. Yin, A. Li, Q. He, B. Li, Targeting PFKL with penfluridol inhibits glycolysis and suppresses esophageal cancer tumorigenesis in an AMPK/FOXO3a/BIM-dependent manner, Acta Pharm. Sin. B 12 (2022) 1271–1287.